

Effects of Nuclear Deformation on the Fusion Probability in the Reactions of $^{76}\text{Ge} + ^{150}\text{Nd}$ and $^{82}\text{Se} + ^{\text{nat}}\text{Ce}$

Katsuhisa Nishio,^{*,a} Hiroshi Ikezoe,^a Shin-ichi Mitsuoka,^a Ken-ichirou Satou,^a and S. C. Jeong^b

^aJapan Atomic Energy Research Institute, Tokai-mura, Naka-gun, Ibaraki 319-1195, Japan

^bInstitute of Particle and Nuclear Studies, KEK, Tsukuba, Ibaraki 305-0801, Japan

Received: December 28, 2001; In Final Form: March 13, 2002

Fusion probabilities for the $^{76}\text{Ge} + ^{150}\text{Nd}$ and $^{82}\text{Se} + ^{\text{nat}}\text{Ce}$ reactions were obtained near the Coulomb barrier, and the effects of nuclear deformation on the fusion process were discussed. The former reaction represents fusion involving the prolately deformed target ^{150}Nd , whereas the latter reaction is the fusion with the spherical target $^{\text{nat}}\text{Ce}$. We obtained the fusion probability by measuring the evaporation residue (ER) cross sections. The system $^{82}\text{Se} + ^{\text{nat}}\text{Ce}$ showed fusion hindrance in the form of the extra-extra-push energy of 27 ± 5 MeV, whereas the system $^{76}\text{Ge} + ^{150}\text{Nd}$ does not show any hindrance at the bombarding energy corresponding to the Coulomb barrier for the collision of ^{76}Ge on the side of ^{150}Nd . Our results suggest that the reaction starting from the compact touching point (side collision) results in a higher fusion probability.

1. Introduction

Synthesis of a super-heavy element (SHE), which is made by heavy ion fusion reactions, is an important and exciting issue for nuclear physics. Because the decay properties of the SHE give information on the shell effects of nucleus, without which such a heavy nucleus could not exist due to overwhelming repulsive Coulomb force. It is generally accepted that the production of evaporation residues comprises of two separate processes, the fusion between two interacting nuclei (entrance channel) and the survival against fission in the course of the de-excitation process (exit channel). The former process is successfully described by a coupled channel model¹ for projectile-target combinations with $Z_1Z_2 \leq 1800$. On the other hand, in heavy systems ($Z_1Z_2 > 1800$), the formation of a compound nucleus is hindered. This is caused by the friction generated between the interacting two nuclei in the course of fusion process. The friction force decreases the kinetic energy of the nuclei, which hinders a complete fusion. To drive the system to the compound nucleus, an additional bombarding energy is needed above the Coulomb barrier to compensate for the energy loss by friction, which is called extra-extra-push energy (E_{XX}). Investigation in References 2–5 showed the E_{XX} to increase sharply with Z_1Z_2 above $Z_1Z_2 \sim 1800$.

Fusion hindrance may be related to the contact point of the interacting two nuclei relative to the fission saddle point of the compound nucleus, from the consideration that the necessary condition for forming a compound nucleus is the dynamical trajectory to pass inside the fission saddle point on the potential energy surface. Simple consideration for the fusion process using two spherical nuclei tells that the distance between mass centers at the contact point expands for heavy systems, which would result in large fusion hindrance. However, even for systems having Z_1Z_2 values larger than 1800, the compact configuration may be achieved by using a prolately deformed target if a projectile collides at the side of the target with $\theta_{\text{coll}} \sim 90^\circ$, where θ_{coll} is the colliding angle of projectile against the symmetry axis of deformed target. We thus expected that the fusion probability using a deformed target is larger than in the system involving spherical nuclei. In order to investigate the effects of nuclear deformation on the fusion process, we have measured the ER cross sections of $^{76}\text{Ge} + ^{150}\text{Nd}$ ($Z_1Z_2 = 1920$)⁶ and $^{82}\text{Se} + ^{\text{nat}}\text{Ce}$ ($Z_1Z_2 = 1972$).⁷ $^{\text{nat}}\text{Ce}$ is spherical in shape, whereas ^{150}Nd is largely deformed with $(\beta_2, \beta_4) = (0.358, 0.107)$.^{8,9} From the experimental data, we determined the fusion probability with

the help of a survival probability determined by a statistical model calculation. The parameters used in this code were determined so as to reproduce the ER cross sections for $^{28}\text{Si} + ^{198}\text{Pt}$ ($Z_1Z_2 = 1092$).⁶

2. Experiments

Measurements of evaporation residue cross sections following the fusion of $^{28}\text{Si} + ^{198}\text{Pt}$, $^{82}\text{Se} + ^{\text{nat}}\text{Ce}$, and $^{76}\text{Ge} + ^{150}\text{Nd}$ were made by using ^{28}Si , ^{82}Se , and ^{76}Ge beam supplied by the JAERI-tandem booster accelerator. The targets were made by sputtering the enriched isotopes (Nd_2O_3 , ^{198}Pt -metal) or $^{\text{nat}}\text{Ce}$ -metal on a 1.5 or 0.8 μm thick aluminum foil. Typical target thickness was 400 $\mu\text{g}/\text{cm}^2$. The target was set to a rotating frame in the target chamber to prevent heating.

Since the evaporation residues produced in the present reaction are α -decaying nuclei, the evaporation channels could be identified by observing α -decay energy and lifetime. The experimental details are described elsewhere.^{6,10} The evaporation residues emitted in beam direction were separated in flight from the primary beam by the JAERI recoil mass separator (JAERI-RMS).¹¹ The separated recoils were implanted into a double sided position-sensitive strip detector (DPSD). Two large area timing detectors, one positioned in front of the DPSD and the other 30 cm upstream of the DPSD, were used to obtain the time-of-flight (TOF) signal of incoming particles. The presence of the TOF signal was used to distinguish ER implantation events from the subsequent α decays, which generate no TOF signals. A two-dimensional spectrum of the energy versus TOF gave a rough estimate of a mass number of the incoming particle, allowing the distinction of ERs from background particles. Typical energy resolution of the DPSD was ~ 70 keV (FWHM). A silicon surface barrier detector to monitor the beams was positioned at 45° direction in the target chamber to determine the absolute values of the ER cross sections.

3. Results

With help of the known α -decay energy and half-life, the identification for a specific channel was made by counting the ER- α_1 - α_2 or ER- α_1 chains, where ER stands for the events produced when the incoming evaporation residue hits the DPSD. α_1 and α_2 are the first and the second correlated α -decay event, respectively. The correlated event satisfied the condition that the position agreement between ER and α event is achieved within $(\Delta X, \Delta Y) = (1.0, 1.0)$ mm. To obtain the absolute ER cross sections, the efficiency of the ER to be transported to the focal plane detector through the JAERI-RMS was evaluated by the method

*Corresponding author. E-mail: nishio@popsvr.tokai.jaeri.go.jp.
FAX: +81-29-282-5927.

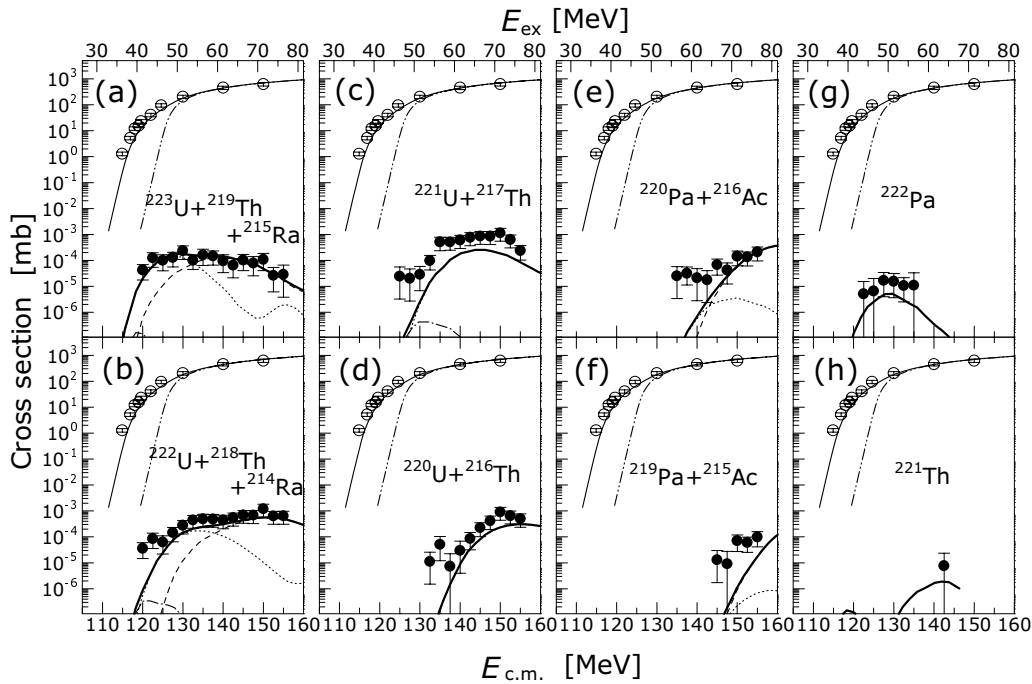


Figure 1. Evaporation residue cross sections for $^{28}\text{Si} + ^{198}\text{Pt}$ (solid circle). Fission cross sections⁶ are also shown (open circle), which are compared to the coupled channel calculation (thin solid curve). Thin dot-dot-dashed curve is the fusion cross section from the one-dimensional barrier penetration model.

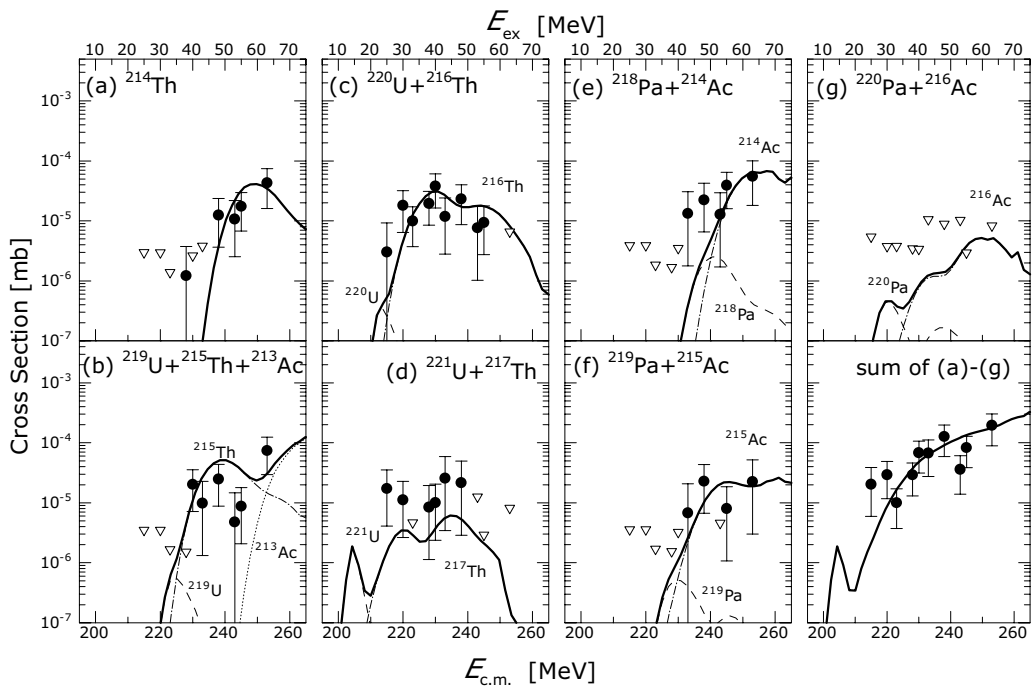


Figure 2. Evaporation residue cross sections for the reaction $^{82}\text{Se} + ^{\text{nat}}\text{Ce}$ (solid circle). Open triangle is the upper limit of the cross section. Thick solid curve is the calculated cross section assuming fusion hindrance in the entrance channel (see text).

described in References 6, 12. We adopted the Shima formula¹³ to estimate the charge distribution.

Evaporation residue cross sections for $^{28}\text{Si} + ^{198}\text{Pt}$, $^{82}\text{Se} + ^{\text{nat}}\text{Ce}$, and $^{76}\text{Ge} + ^{150}\text{Nd}$ are shown in Figure 1, 2, and 3, respectively, as a function of the c.m. energy (and also excitation energy E_{ex}) by solid circles with error bars. Note that Figure 3(a) for $^{76}\text{Ge} + ^{150}\text{Nd}$ contains $1n$ (^{225}U) and $2n$ (^{224}U) channels. The error includes both statistical contributions and the estimated uncertainty of 50% coming from the ambiguity in transport efficiency of ERs through the JAERI-RMS.

4. Analysis and Discussion

The experimental ER cross section $\sigma_{\text{er},c}$ for the observed channel c was used to obtain the fusion probability weighted

by the angular momentum l by

$$P_{\text{fus}}(E_{\text{c.m.}}) = \frac{\sum_c \sigma_{\text{er},c}(E_{\text{c.m.}})}{\pi \lambda^2 \sum_l (2l+1) \sum_c w_{\text{er},c}(E_{\text{c.m.}} + Q, l)}. \quad (1)$$

The survival probability $w_{\text{er},c}$ against fission for the channel c is a function of the excitation energy $E_{\text{ex}} = E_{\text{c.m.}} + Q$ (reaction Q value) and the angular momentum l . This was calculated by the statistical model calculation (HIVAP code¹⁴).

Parameters used in the HIVAP code were determined by measuring the ER and the fission cross sections for $^{28}\text{Si} + ^{198}\text{Pt}$ (Ref. 6). This is the light fusion system with $Z_1 Z_2 = 1092$ and is expected to have no fusion hindrance. The fusion cross section (Figure 1), which is approximated to the fission cross section for this reaction, was calculated by the coupled channel calculation (CCDEF code¹⁵). We took into account the nuclear deformation of ^{28}Si ($\beta_2 = 0.407^{16}$) and ^{198}Pt ($\beta_2 = -0.060$,⁸

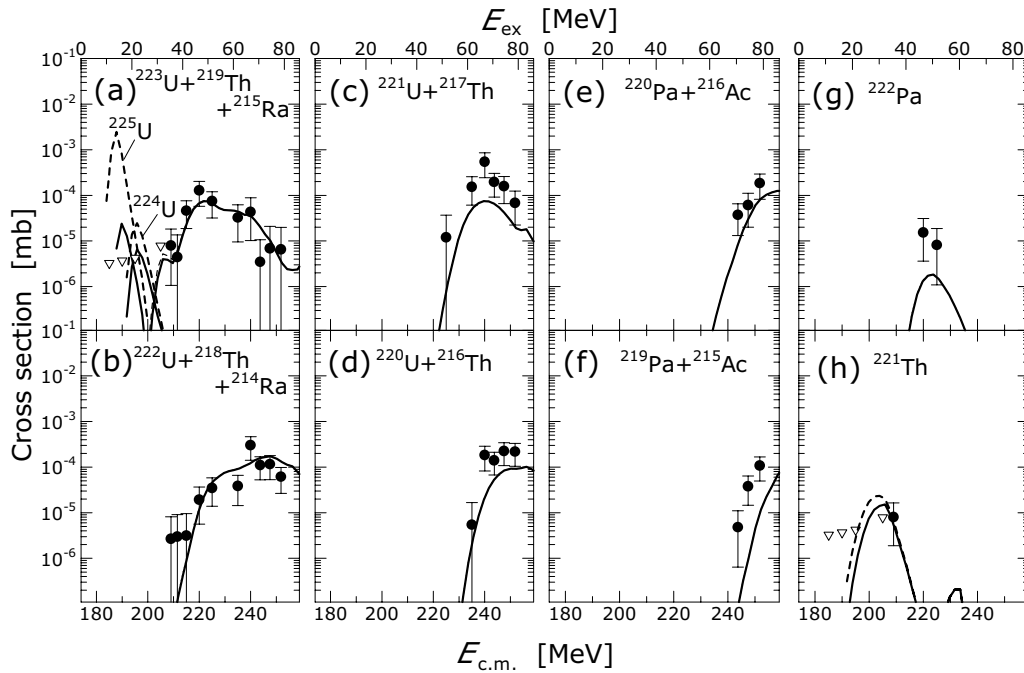


Figure 3. Evaporation residue cross sections for the reaction $^{76}\text{Ge} + ^{150}\text{Nd}$ (solid circle).

$\beta_4 = -0.030^9$) as well as the couplings of the octupole (3-) vibrational states in ^{28}Si ($\beta_3 = 0.398$, 6.88 MeV)¹⁷ and ^{198}Pt ($\beta_3 = 0.050$, 1.68 MeV).¹⁷ It is found in Figure 1 that the CCDEF calculation reproduces the fission cross section quite well down to the sub-barrier energy region. The corresponding partial wave distribution was put to the HIVAP code to obtain the ER cross sections. By assuming HIVAP parameters described in References 6, 10, the ER cross sections for each channels are obtained and shown in Figure 1 (thick solid curve). The calculation nicely reproduced the experimental cross sections, indicating the validity of our parametrization. The fusion probability for $^{28}\text{Si} + ^{198}\text{Pt}$ was calculated by eq 1, and the results are shown in Figure 4 as a function of $E_{c.m.}/V_B$, where $V_B = 125.5$ MeV is the spherical Coulomb barrier for this reaction. Above this barrier P_{fus} is almost constant and has the value 1.

The resulting fusion probability for $^{82}\text{Se} + ^{\text{nat}}\text{Ce}$ is shown in Figure 4 as a function of $E_{c.m.}/V_B$, where V_B is taken as

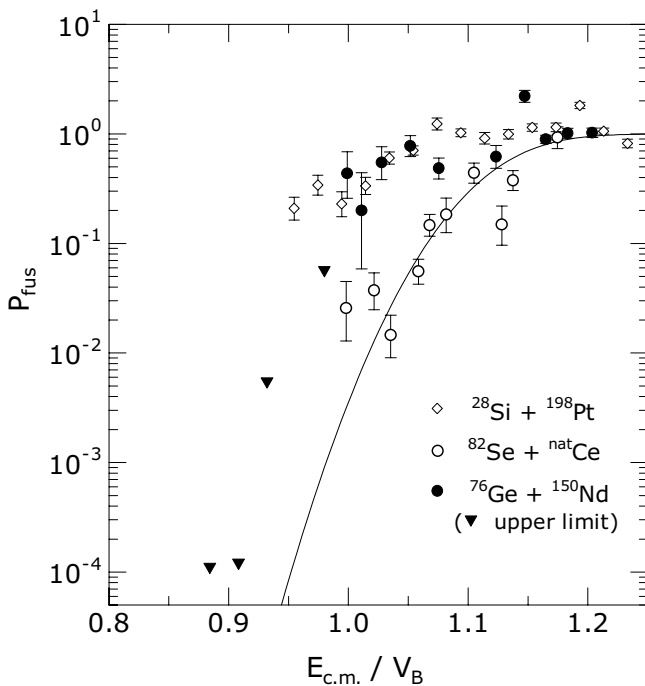


Figure 4. Fusion probability for $^{28}\text{Si} + ^{198}\text{Pt}$, $^{82}\text{Se} + ^{\text{nat}}\text{Ce}$, and $^{76}\text{Ge} + ^{150}\text{Nd}$.

215.3 MeV of $^{82}\text{Se} + ^{140}\text{Ce}$. Below $E_{c.m.}/V_B = 1.15$, P_{fus} for $^{82}\text{Se} + ^{\text{nat}}\text{Ce}$ decreases considerably with lowering the bombarding energy, showing the curve similar to the massive system having fusion hindrance.^{2,4,5} By finding the $E_{c.m.}$ at which P_{fus} of $^{82}\text{Se} + ^{\text{nat}}\text{Ce}$ crosses the $P_{\text{fus}} = 0.5$ level, we obtained the extra-extra-push energy $E_{\text{XX}} = 27 \pm 5$ MeV for this reaction.

Fusion probability for massive system can be represented by assuming the fusion barrier distribution to have Gaussian in shape.^{4,5} By setting the center of the barrier as $V_B + E_{\text{XX}}$ ($E_{\text{XX}} = 25$ MeV) and the standard deviation of $\sigma_B = 10$ MeV, we could describe the P_{fus} for $^{82}\text{Se} + ^{\text{nat}}\text{Ce}$ as shown in Figure 4 (solid curve). The corresponding partial wave cross section was calculated and implemented to the HIVAP code as an initial spin distribution, and the ER cross section was calculated as shown in Figure 2. The calculation reproduces the experimental ER cross sections.

The fusion probability P_{fus} for $^{76}\text{Ge} + ^{150}\text{Nd}$ is shown in Figure 4 by the solid circles with statistical error bars. P_{fus} values of $^{76}\text{Ge} + ^{150}\text{Nd}$ are nearly flat with ~ 1.0 down to $E_{c.m.} \sim V_B$ ($= 209$ MeV) given by assuming the ^{150}Nd nucleus to be spherical (spherical Coulomb barrier). This trend is similar to the fusion of $^{28}\text{Si} + ^{198}\text{Pt}$ which exhibits no fusion hindrance, and the excitation function shows marked contrast to that of $^{82}\text{Se} + ^{\text{nat}}\text{Ce}$. It is apparent that the reaction $^{76}\text{Ge} + ^{150}\text{Nd}$ exhibits no fusion hindrance at and above the spherical Coulomb barrier. We did not observe any events at $E_{c.m.} < V_B$ and thus the upper limit is shown by the solid reversed-triangle in Figure 4.

Because of the large deformation of ^{150}Nd , the fusion barrier for $^{76}\text{Ge} + ^{150}\text{Nd}$ distributes widely. We have calculated the fusion cross section for $^{76}\text{Ge} + ^{150}\text{Nd}$ by the coupled-channel model (CCDEF code¹⁵). The important characteristic in this reaction is that the Coulomb barrier height is nearly constant with 210 ~ 214 MeV in the side collision of $50^\circ \sim 90^\circ$ as a result of the ^{150}Nd deformation ($\beta_2 = 0.358$, $\beta_4 = 0.107$). The partial wave cross sections from CCDEF code were inputted to the HIVAP code to yield ER cross sections. It was found that the calculated cross sections for the energy range of $185 < E_{c.m.} < 195$ MeV lie far above the upper limit of the experimental data of the ^{225}U channel as indicated by the dashed line in Figure 3(a). This indicates that the system does not fuse if the projectile collides with the tip of the prolatelly deformed target of ^{150}Nd when the bombarding energy is set to the corresponding Coulomb barrier (184 MeV). The experimental data was reproduced only

when the extra-extra-push energy was assumed for the tip collision. The barrier height was effectively enhanced assuming that the shift is linearly scaled with the Coulomb barrier distance (r) and has the maximum value at the tip collision ($\theta_{\text{coll}} = 0^\circ$, $E_{\text{XX0}} = 13$ MeV) and the minimum at the side collision ($\theta_{\text{coll}} = 90^\circ$, $E_{\text{XX}} = 0$ MeV) as

$$E_{\text{XX}}(r) = E_{\text{XX0}} \frac{r - R_{\text{side}}}{R_{\text{tip}} - R_{\text{side}}}. \quad (2)$$

Note that the Coulomb barrier distance r , determined by the CCDEF code, is a function of θ_{coll} . R_{side} and R_{tip} becomes 11.7 and 14.6 fm, respectively. As seen in Figure 3, the ER cross sections of the ^{225}U channel decreases by two orders magnitude and is consistent with the experiment. For the bombarding energy of the side collision (210 ~ 214 MeV), the experimental ER cross sections are reproduced in the calculation, supporting that there is no fusion hindrance at the side collision for $^{76}\text{Ge} + ^{150}\text{Nd}$.

The side collision ($\theta = 90^\circ$) for $^{76}\text{Ge} + ^{150}\text{Nd}$ gives a Coulomb barrier distance of 11.7 fm, which is smaller than the distance for $^{82}\text{Se} + ^{140}\text{Ce}$ (12.3 fm). If we assume that the fission saddle points do not differ very much in the two systems (^{222}U for $^{82}\text{Se} + ^{140}\text{Ce}$ and ^{226}U for $^{76}\text{Ge} + ^{150}\text{Nd}$), it can be considered that the configuration of the side collision of $^{76}\text{Ge} + ^{150}\text{Nd}$ is close to the fission saddle point. Thus the loss in kinetic energy in the fusion process is minimized and is smaller than for $^{82}\text{Se} + ^{140}\text{Ce}$. We also want to mention that the tip collision of ^{76}Ge on ^{150}Nd has the Coulomb barrier distance of $R_{\text{tip}} = 14.6$ fm, which is larger than that of $^{82}\text{Se} + ^{\text{nat}}\text{Ce}$. The long distance would result in a large amount of kinetic energy needed to form the compound nucleus.

5. Conclusions

Evaporation residue cross sections for $^{76}\text{Ge} + ^{150}\text{Nd}$ and $^{82}\text{Se} + ^{\text{nat}}\text{Ce}$ were measured in the vicinity of the Coulomb barrier. We also measured the ER and fission cross sections for $^{28}\text{Si} + ^{198}\text{Pt}$ to determine the parameters used in the statistical model calculation, yielding the survival probability in the exit channel. The fusion of $^{82}\text{Se} + ^{\text{nat}}\text{Ce}$ is a reaction characterized by spherical colliding partners with $Z_1 Z_2 = 1972$. The fusion hindrance was observed in the form of extra-extra-push energy 27 ± 5 MeV. For the reaction $^{76}\text{Ge} + ^{150}\text{Nd}$, which has $Z_1 Z_2 = 1920$ being close to $^{82}\text{Se} + ^{\text{nat}}\text{Ce}$, the obtained fusion probability did not exhibit any fusion hindrance at all for the side collision of $50^\circ < \theta_{\text{coll}} < 90^\circ$. It therefore can be concluded that the compact touching configuration promotes fusion even for massive system with $Z_1 Z_2 > 1800$. This idea is supported by the experimental results that for the tip collision of ^{76}Ge on ^{150}Nd

the large Coulomb barrier distance caused fusion hindrance and resulted in an extra-extra-push energy for the system to form a compound nucleus.

Acknowledgment. We would like to thank the crew of the JAERI tandem accelerator for generating ^{28}Si , ^{76}Ge , and ^{82}Se beams.

References

- (1) A. B. Balantekin and N. Takigawa, *Rev. Mod. Phys.* **70**, 77 (1998).
- (2) J. G. Keller, K.-H. Schmidt, F. P. Hessberger, G. Münzenberg, W. Reisdorf, H.-G. Clerc, and C.-C. Sahn, *Nucl. Phys. A* **452**, 173 (1986).
- (3) C.-C. Sahn, H.-G. Clerc, K.-H. Schmidt, W. Reisdorf, P. Armbruster, F. P. Hessberger, J. G. Keller, G. Münzenberg, and D. Vermeulen, *Z. Phys. A* **319**, 113 (1984).
- (4) C.-C. Sahn, H.-G. Clerc, K.-H. Schmidt, W. Reisdorf, P. Armbruster, F. P. Hessberger, J. G. Keller, G. Münzenberg, and D. Vermeulen, *Nucl. Phys. A* **441**, 316 (1985).
- (5) A. B. Quint, W. Reisdorf, K.-H. Schmidt, P. Armbruster, F. P. Hessberger, S. Hofmann, J. Keller, G. Münzenberg, H. Stelzer, H.-G. Clerc, W. Morawek, and C.-C. Sahn, *Z. Phys. A* **346**, 119 (1993).
- (6) K. Nishio, H. Ikezoe, S. Mitsuoka, and J. Lu, *Phys. Rev. C* **62**, 014602 (2000).
- (7) K. Nishio, H. Ikezoe, S. Mitsuoka, K. Satou, and S. C. Jeong, *Phys. Rev. C* **63**, 044610 (2001).
- (8) P. Raghavan, *At. Data Nucl. Data Tables* **42**, 189 (1989).
- (9) P. Möller, J. R. Nix, W. D. Myers, and W. J. Swiatecki, *At. Data Nucl. Data Tables* **59**, 185 (1995).
- (10) S. Mitsuoka, H. Ikezoe, K. Nishio, and J. Lu, *Phys. Rev. C* **62**, 054603 (2000).
- (11) H. Ikezoe, Y. Nagame, T. Ikuta, S. Hamada, I. Nishinaka, and T. Ohtsuki, *Nucl. Instrum. Methods A* **376**, 420 (1996).
- (12) T. Kuzumaki, H. Ikezoe, S. Mitsuoka, T. Ikuta, S. Hamada, Y. Nagame, I. Nishinaka, and O. Hashimoto, *Nucl. Instrum. Methods A* **437**, 107 (1999).
- (13) K. Shima, T. Ishihara, and T. Mikuno, *Nucl. Instrum. Methods* **200**, 605 (1982).
- (14) W. Reisdorf and M. Schädel, *Z. Phys. A* **343**, 47 (1992).
- (15) J. O. Fernández Niello, C. H. Dasso, and S. Landowne, *Comput. Phys. Commun.* **54**, 409 (1989).
- (16) M. Dasgupta, A. Navin, Y. K. Agarwal, C. V. K. Baba, H. C. Jain, and M. L. Jhingan, *Nucl. Phys. A* **539**, 351 (1992).
- (17) R. H. Spear, *At. Data Nucl. Data Tables* **42**, 55 (1989).